Analysis of effects of macroscopic propagation and multiple molecular orbitals on the minimum in high-order harmonic generation of aligned CO_2

Cheng Jin, Anh-Thu Le, and C. D. Lin
J. R. Macdonald Laboratory, Physics Department, Kansas State University, Manhattan, Kansas 66506-2604, USA
(Received 14 March 2011; published 9 May 2011)

We report theoretical calculations of the effect of the multiple-orbital contribution in high-order harmonic generation (HHG) of aligned CO_2 with the inclusion of macroscopic propagation of harmonic fields in the medium. Our results show very good agreement with recent experiments for the dynamics of the minimum in HHG spectra as laser intensity or alignment angle changes. Calculations are carried out to check how the position of the minimum in HHG spectra depends on the degrees of molecular alignment, laser-focusing conditions, and the effects of alignment-dependent ionization rates of the different molecular orbitals. These analyses help to explain why the minima observed in different experiments may vary.

DOI: 10.1103/PhysRevA.83.053409 PACS number(s): 33.80.Rv, 42.65.Ky, 31.70.Hq, 33.80.Eh

I. INTRODUCTION

High-order harmonic generation (HHG) emitted when atoms or molecules are exposed to an intense laser field [1–3] is one of the most interesting nonlinear phenomena. Experimentally, the harmonic fields generated by all atoms or molecules within the laser focus copropagate with the fundamental laser field until they reach the detector. To compare with experimental measurements, theoretical harmonics from each atom or molecule first have to be calculated. The induced dipoles are then fed into the propagation equation, taking into account the focusing condition and the nature of the gas medium, and the equation is finally integrated until the harmonics are collected [4–8].

HHG from randomly distributed molecules has been studied since the 1990s [9–12]. In recent years, experimental HHG studies have tended to focus on partially aligned molecules [13–16]. Among the molecules, CO_2 is likely the most extensively studied system so far [17–20], with the interest initially focused on the observation of the minimum in the HHG spectra [21–23]. The positions of the minima from different experiments, however, are often vastly different. According to the three-step model [24,25], HHG is generated through the recombination of the returning electrons with the molecular ion. The interference of electron waves from the two atomic centers, under some conditions, results in a minimum in the transition dipole; the simplest analysis is the two-center interference model [26–28]. In fact, recombination is an inverse process of photoionization. Thus the transition dipole is the same as that in photoionization. Any such minima have not been observed in photoionization, however, since in these measurements molecules are isotropically distributed.

On the theoretical side, the alignment dependence of HHG was first studied using the strong-field approximation (SFA) (or the Lewenstein model) [29–31]. Subsequently we developed a quantitative rescattering (QRS) theory [32–34] for HHG, which was a significant improvement on the Lewenstein model. In QRS, the accuracy of recombination is treated at the same level as in the photoionization process. Using QRS, the HHG minimum is attributed to the minimum in the photoionization transition dipole between the highest occupied molecular orbital (HOMO) and continuum molecular wave functions [34,35]. For fixed-in-space CO_2 molecules, the photoionization cross sections of the HOMO indeed exhibit minima at small alignment angles. The experimental HHG spectra from partially aligned CO_2 have been explained reasonably well by QRS, including the harmonic intensities and the phase, as well as the polarization and ellipticity of the harmonics [35,36].

If HHG is generated from the HOMO only, then one expects that the position of the minimum does not significantly change with laser intensity, according to QRS theory. Indeed, strong-field ionization depends exponentially on the ionization potential I_p. The HOMO-1 and HOMO-2 orbitals in CO_2 are more deeply bound by 4 and 4.4 eV, respectively, than the HOMO [37], thus they are not expected to contribute significantly to the HHG spectra. However, it is also well known that tunneling ionization rates depend sensitively on the symmetry of the molecular orbital [38]. The HOMO is a π_g orbital. This means that at small alignment angles, the ionization rates are small. For HOMO-2, however, it is a σ_g orbital, therefore it has a large ionization rate when CO_2 molecules are parallel aligned. Thus for small alignment angles, the HOMO-2 may become important even though it is bound 4.4-eV deeper than the HOMO. (The HOMO-1 is a π_u orbital and thus not expected to contribute significantly to the HHG.)

The first step of the HHG process is tunneling ionization. The alignment dependence of the tunneling ionization rate is usually calculated using the molecular Ammosov-Delone-Krainov (MO-ADK) theory [39,40] or SFA. For most molecules that have been studied, these two models give nearly identical alignment dependence (after normalization). However, this is not the case for CO_2. Experimentally, the alignment dependence of CO_2 ionization reported by Pavičić *et al.* [41] is very narrowly peaked near the alignment angle of 46°. It differs significantly from the predictions of the MO-ADK theory and SFA [42]. In fact, so far all theoretical attempts [43–47] have been unable to confirm the sharp alignment dependence reported in the experiment. Furthermore, the observed HHG spectra from aligned molecules are inconsistent with the reported experimental alignment dependence of ionization [36,48].

The HHG spectra of parallel aligned CO_2 have been studied in a number of experiments, with 800-nm lasers [21] as well as lasers of longer wavelengths [23,49]. It was

observed that the position of the HHG minimum moved to higher photon energies as laser intensity was increased. In Smirnova *et al.* [21], such effects were interpreted in terms of the multichannel interference (between the HOMO and HOMO-2) and the intricate hole dynamics. Their calculations were based on HHG generated by a single-molecule response. They introduced filters into the theory such that only short trajectories contributed to the signals. In their calculation, a relative phase between different channels due to a strong-field ionization step was introduced "by hand" in order to obtain the good agreement with the measurement.

As noted at the beginning, to compare theoretically simulated HHG spectra of molecules with experimental ones, the effect of macroscopic propagation should be considered. Practically, this has rarely been done. For atomic targets, the propagation effect is usually included with single-atom induced dipoles calculated using the Lewenstein model. Only on a few rare occasions has the atomic response been calculated more accurately by solving the time-dependent Schrödinger equation (TDSE) [50,51]. It is also well known that the Lewenstein model does not predict the HHG spectra (the intensity) precisely, but the phases of the harmonics are relatively accurate. This fact is used in the QRS model, which can be understood as simply replacing the transition dipole calculated using plane waves in the Lewenstein model with one calculated using accurate molecular continuum wave functions. The improvement of single-molecule HHG spectra calculated using QRS has been well documented in our previous papers [34,52]. Computationally, QRS is nearly as simple as the Lewenstein model (actually QRS is even simpler than SFA for polyatomic molecules; see Ref. [53]), thus the induced dipole can be easily obtained from QRS to feed into the propagation equations to account for medium propagation effects. This has been done for atomic targets with conditions of low laser intensity and low gas pressure [54]. It has been extended recently to the conditions of high intensity and high pressure for Ar and to molecular targets [8,55], including polyatomic molecules [53].

In this paper, we report theoretical studies of the propagation effect on the HHG of CO_2, including contributions from the HOMO and HOMO-2. Note that, experimentally, the effect of propagation on the HHG spectra has rarely been investigated, in particular, its effect on the minimum of the HHG spectra. However, this has changed recently with reports of such studies on Ar [55–57]. The rest of this paper is arranged as follows. In Sec. II, we first summarize the equations used for the propagation calculations. We limit ourselves to low laser intensity and low pressure. To extend the theory to high intensity and high pressure, the optical properties of CO_2 have to be used, which are not available over a broad range of frequencies. We then summarize how the single-molecule response from partially aligned molecules is calculated. In Sec. III, the calculated results are presented. Different factors that can influence the precise positions of the HHG minima are examined and reported. These results show that precise theoretical predictions of the positions of HHG minima in a given experiment are difficult, but the trend (the direction of the shift of the minimum positions) can be predicted (or explained). A short summary at the end concludes this paper.

II. THEORETICAL METHOD

We first briefly describe the theory of propagation of high harmonics in a macroscopic medium, and in free space, until they reach the detector. To calculate the induced dipole for individual molecules, we include the contributions from multiple molecular orbitals. Our method is based on extending the QRS theory [34].

A. Propagation of harmonics in the medium

In general, both the fundamental laser field and the harmonic field are modified when they copropagate through a macroscopic medium. In this paper, we limit ourselves to experiments carried out under the conditions of low laser intensity and low gas pressure, where the effects of dispersion, Kerr nonlinearity, and plasma defocusing on the fundamental laser field can be neglected [8,54]. The fundamental laser field is assumed to be a Gaussian beam in space. Its spatial and temporal dependence can be expressed in an analytical form [54]. For high harmonics, dispersion and absorption effects from the medium are not included. The dispersion and absorption coefficients depend linearly on gas pressure and could be ignored under low pressure [8]. The free-electron dispersion is also neglected, since the plasma frequency is much smaller than the frequencies of high harmonics [5].

The three-dimensional propagation equation of the harmonic field is described as [4–6,8,54]

$$\nabla_\perp^2 \tilde{E}_{\rm h}^{\parallel}(r,z',\omega,\alpha) - \frac{2i\omega}{c}\frac{\partial \tilde{E}_{\rm h}^{\parallel}(r,z',\omega,\alpha)}{\partial z'} = -\omega^2\mu_0 \tilde{P}_{\rm nl}^{\parallel}(r,z',\omega,\alpha), \quad (1)$$

where

$$\tilde{E}_{\rm h}^{\parallel}(r,z',\omega,\alpha) = \hat{F}[E_{\rm h}^{\parallel}(r,z',t',\alpha)], \quad (2)$$

and

$$\tilde{P}_{\rm nl}^{\parallel}(r,z',\omega,\alpha) = \hat{F}[P_{\rm nl}^{\parallel}(r,z',t',\alpha)]. \quad (3)$$

Here $\hat{F}$ is the Fourier-transform operator acting on the temporal coordinate. Equation (1) is written in a moving coordinate frame ($z' = z$ and $t' = t - z/c$), and the term $\partial^2 E_{\rm h}^{\parallel}/\partial z'^2$ is neglected. $\tilde{E}_{\rm h}^{\parallel}(r,z',\omega,\alpha)$ is the parallel component of the harmonic field with respect to the polarization direction of the probe (or generating) laser, and $\tilde{P}_{\rm nl}^{\parallel}(r,z',\omega,\alpha)$ is the parallel component of the nonlinear polarization caused by the generating laser field, where α is the pump-probe angle, i.e., the angle between the aligning laser and the harmonic-generating laser polarizations.

The nonlinear polarization term can be expressed as

$$\tilde{P}_{\rm nl}^{\parallel}(r,z',\omega,\alpha) = \hat{F}\{[n_0 - n_{\rm e}(r,z',t',\alpha)]D^{\parallel,\rm tot}(r,z',t',\alpha)\}, \quad (4)$$

where n_0 is the density of neutral molecules, $D^{\parallel,\rm tot}(t',\alpha)$ is the parallel component of the induced single-molecule dipole over a number of active electrons [see Eq. (12) below], and $n_{\rm e}(t',\alpha)$ is the free-electron density, which can be calculated as follows:

$$n_{\rm e}(t',\alpha) = \int_0^\pi n_{\rm e}(t',\theta)\rho(\theta,\alpha)\sin\theta d\theta. \quad (5)$$

Here, $n_e(t',\theta)$ is the alignment-dependent free-electron density obtained from

$$n_e(t',\theta) = n_0\left\{1 - \exp\left[-\int_{-\infty}^{t'} \gamma(\tau,\theta)d\tau\right]\right\}, \quad (6)$$

where $\gamma(\tau,\theta)$ is the alignment-dependent ionization rate, which can be calculated by the MO-ADK theory [39,40] for different molecular orbitals. In Eq. (5), θ is the alignment angle with respect to the polarization direction of the probe laser, and $\rho(\theta,\alpha)$ is the alignment distribution with pump-probe angle α [34,58,59].

After the propagation in the medium, we obtain the parallel component of near-field harmonics on the exit face of the gas jet ($z' = z_{\text{out}}$). For isotropically distributed molecules and partially aligned molecules with $\alpha = 0^\circ$ or 90°, by symmetry there are only parallel harmonic components. The perpendicular components, which are usually much smaller, would appear for partially aligned molecules and the harmonics would be elliptically polarized in general [36]. The generalization of Eq. (1) to the perpendicular component is straightforward, but we restrict ourselves to the parallel component only. Equation (1) is solved numerically using a Crank-Nicholson routine for each value of ω. Typical parameters used in the calculations are 300 grid points along the radial direction and 400 grid points along the longitudinal direction.

B. Harmonics in the far field

Once the near-field harmonics are obtained on the exit face of the medium, they further propagate in free space before detection by the spectrometer. Meanwhile, they may pass through a slit, an iris, or be reflected by a mirror. The far-field harmonics can be obtained from near-field harmonics through a Hankel transformation [60–62],

$$E_h^f(r_f,z_f,\omega,\alpha) = -ik\int \frac{\tilde{E}_h^{\parallel}(r,z',\omega,\alpha)}{z_f - z'} J_0\left(\frac{krr_f}{z_f - z'}\right) \times \exp\left[\frac{ik\left(r^2 + r_f^2\right)}{2(z_f - z')}\right] rdr, \quad (7)$$

where J_0 is the zero-order Bessel function, and z_f and r_f are the coordinates of the far-field points. The wave vector k is given by $k = \omega/c$.

We assume that the harmonics in the far field are collected from an extended area. By integrating harmonic yields over the area, the power spectrum of the macroscopic harmonics is obtained by

$$S_h(\omega,\alpha) \propto \int\int \left|E_h^f(x_f,y_f,z_f,\omega,\alpha)\right|^2 dx_f dy_f, \quad (8)$$

where x_f and y_f are the Cartesian coordinates on the plane perpendicular to the propagation direction, and $r_f = \sqrt{x_f^2 + y_f^2}$. To simulate experimental HHG spectra quantitatively, besides laser parameters, detailed information on the experimental setup is needed.

C. Quantitative rescattering theory for a multi-orbital molecular system

In Eq. (4), laser-induced single-molecule dipole moment $D(t')$ is calculated quantum mechanically using the QRS theory, which has been discussed in detail for molecules in Ref. [34]. Within QRS, laser-induced dipole moment $D(\omega,\theta)$ for a molecule at a fixed angle θ (measured with respect to laser polarization) is given by

$$D^{\parallel,\perp}(\omega,\theta) = N(\theta)^{1/2}W(\omega)d^{\parallel,\perp}(\omega,\theta), \quad (9)$$

where $N(\theta)$ is the alignment-dependent ionization probability, $W(\omega)$ is the recombining electron wave packet, and $d^{\parallel,\perp}(\omega,\theta)$ is the parallel component (or perpendicular component) of the photorecombination (PR) transition dipole (complex in general). Here we only consider linearly polarized lasers and linear molecules. $W(\omega)$ is independent of the alignment angle θ. From Eq. (9), it can be expressed as

$$W(\omega) = \frac{D^{\parallel,\perp}(\omega,\theta)}{N(\theta)^{1/2}d^{\parallel,\perp}(\omega,\theta)}. \quad (10)$$

In QRS, $W(\omega)$ is usually calculated only once for a given angle θ using SFA, where all the elements on the right-hand side of Eq. (10) are obtained by replacing the continuum waves with plane waves. In QRS, accurate $d^{\parallel,\perp}(\omega,\theta)$ are obtained from quantum chemistry code [63,64] and tunneling ionization probability $N(\theta)$ are obtained either from the MO-ADK theory [39,40] or from SFA. When all of these are put together in Eq. (9), the laser-induced dipole moment $D(\omega,\theta)$ for each orbital is obtained. Note that in QRS, the wave packet $W(\omega)$ automatically includes the phase which is dependent on the molecular orbital. Thus there is no need to introduce the relative phase between orbitals, in contrast to the approach in Ref. [21]. SFA is used to calculate the ionization probability in Eq. (9) in this paper, unless otherwise stated.

We assume that the degree of molecular alignment is not varied spatially within the medium because the molecules are usually partially aligned by a weak and loosely focused laser beam [58]. By coherently averaging the induced dipole moments over the molecular angular distribution, we obtain the averaged induced dipole of partially aligned molecules at each point inside the medium:

$$D^{\parallel,\text{avg}}(\omega,\alpha) = \int_0^\pi D^{\parallel}(\omega,\theta)\rho(\theta,\alpha)\sin\theta d\theta, \quad (11)$$

where $\rho(\theta,\alpha)$ is again the angular (or alignment) distribution of the molecules with respect to the polarization direction of the probe laser. For randomly distributed molecules, $\rho(\theta,\alpha)$ is a constant. Note that the above procedure is only for the specified molecular orbital.

For the specific problem addressed in this paper, we consider electrons either in the HOMO ($1\pi_g$) or in the HOMO-2 ($3\sigma_u$) of CO_2. The electrons are freed and then recombine back to the same orbital. As discussed above, the multiple orbital effects are important at small alignment angles only due to symmetry consideration. At these angles, the HOMO-1 ($1\pi_u$) is ignored since the ionization rate of

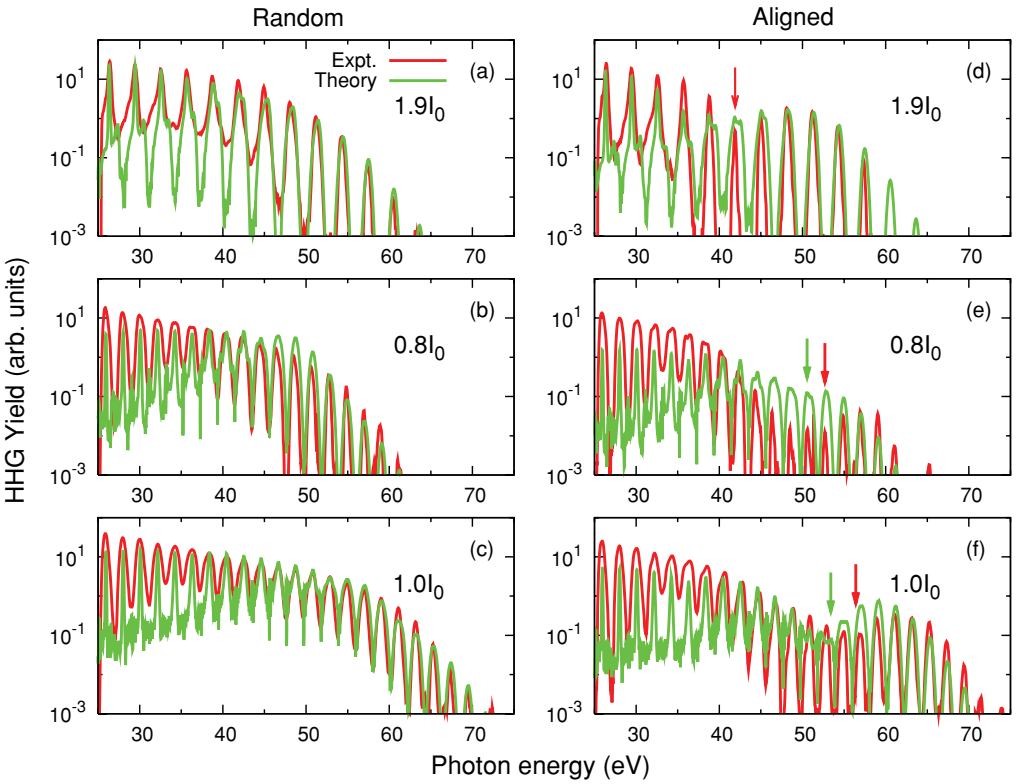

FIG. 1. (Color online) Comparison of theoretical [green (light gray) lines] and experimental [red (dark gray) lines] HHG spectra of random and aligned CO_2 molecules in (a), (d) an 800-nm laser and (b), (c), (e), (f) a 1200-nm laser. Laser intensities are indicated where $I_0 = 10^{14}$ W/cm^2. Experimental data are from Ref. [49]. Arrows indicate the positions of minima. Pump-probe angle $\alpha = 0^\circ$. See text for additional laser parameters and experimental arrangements.

the HOMO-1 is quite small compared with the HOMO and HOMO-2 [21,40,43]. At large alignment angles, only the HOMO becomes important. The total laser-induced dipole over a number of active electrons can be written as [65,66]

$$D^{\parallel,\mathrm{tot}}(\omega,\alpha) = \sum_{j,n} D^{\parallel,\mathrm{avg}}_{j,n}(\omega,\alpha), \tag{12}$$

where index j refers to the HOMO and HOMO-2 of CO_2, and n is an index to account for degeneracy in each molecular orbital.

Before proceeding, we comment that the QRS theory is formulated in the energy (or frequency) domain. There is no explicit treatment of "core dynamics" as in Ref. [21]. The time evolution of the core is reflected only by the energy of the core in the free propagation of the electron wave packet. In other words, any possible many-body interchannel couplings between the HOMO and HOMO-2 are not included in the present treatment. Before such effects are addressed, other factors that are more important to the HHG as discussed here have to be treated first.

For the propagation of harmonics in the medium, we need to obtain hundreds of total induced dipoles $D^{\parallel,\mathrm{tot}}(\omega,\alpha)$ for different laser intensities, which are then fed into Eq. (1). The same procedure is used in Jin *et al.* [54] for atomic targets. Note that in the present model, the dielectric properties of molecules due to nonisotropic distributions are also neglected.

III. RESULTS AND DISCUSSION

A. HHG spectra of randomly distributed CO_2: Theory versus experiment

HHG spectra by 800-nm and 1200-nm lasers have been reported for isotropically distributed and partially aligned N_2 and CO_2 molecules [49]. The spectra of N_2 have been analyzed by Jin *et al.* [8,55] recently, including only the HOMO.

In Figs. 1(a)–1(c), we show the HHG spectra for isotropically distributed CO_2 molecules by 800-nm and 1200-nm lasers. To obtain good agreement between theory and experiment, especially in the cutoff region, the intensity used in the theory is adjusted from the value given in the experiment. In Figs. 1(a)–1(c), the intensities in theory (experiment) are 1.9 (2.1), 0.8 (1.0), and 1.0 (1.2), in units of 10^{14} W/cm^2, respectively. Other parameters used in the simulation are the same as those given in the experiment [49]. The laser parameters are pulse duration of ∼32 fs (800 nm) or ∼44 fs (1200 nm), and beam waist at the focus of ∼40 μm. A 0.6-mm-wide gas jet is located 3 mm (800 nm) or 3.5 mm (1200 nm) after the laser focus, and a slit with a width of 100 μm is placed at 24 cm after the gas jet.

Figures 1(a)–1(c) clearly show the good overall agreement between experiment and theory for randomly distributed CO_2 molecules. We have checked that the HOMO is dominant for randomly distributed CO_2, with negligible contributions from inner orbitals. The HHG spectra do not exhibit any minima, as opposed to the spectra of random N_2 molecules

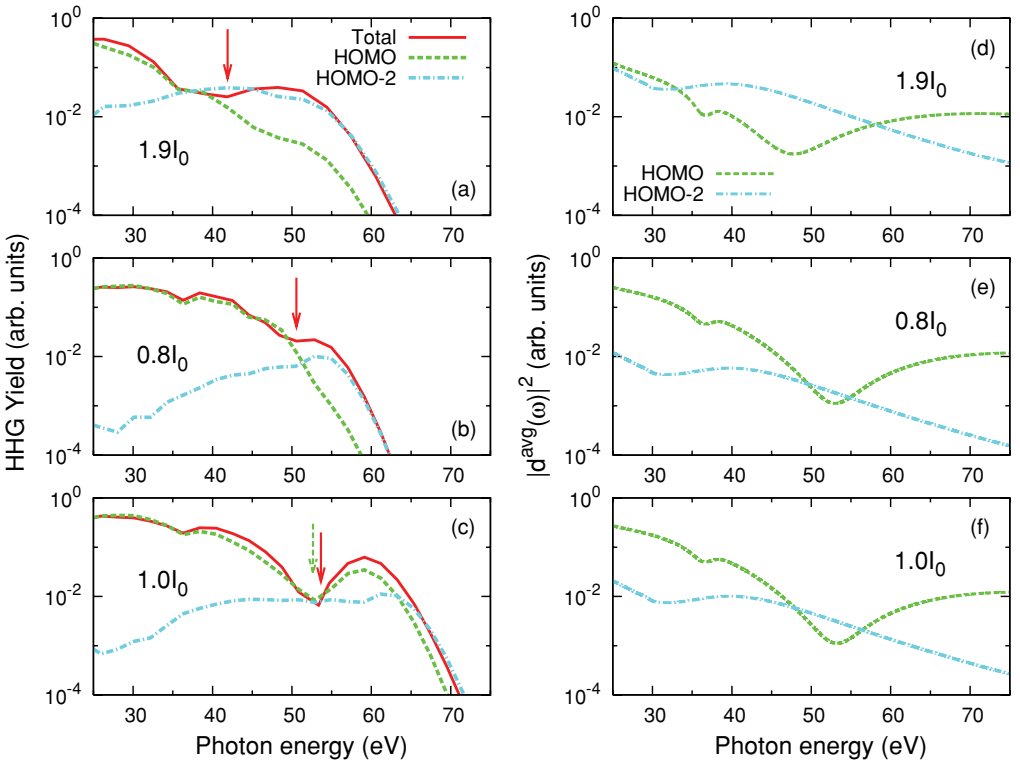

FIG. 2. (Color online) (a)–(c) Macroscopic HHG spectra (envelope only) corresponding to Figs. 1(d)–1(f), respectively. Total (HOMO and HOMO-2 together) spectra and the spectra of the individual HOMO and HOMO-2 are shown. (d)–(f) Averaged photorecombination transition dipoles (parallel component, the square of magnitude) of the HOMO and HOMO-2 corresponding to (a), (b), and (c), respectively. Laser intensities are indicated where $I_0 = 10^{14}$ W/cm^2. Arrows indicate the positions of minima. Pump-probe angle $\alpha = 0^\circ$.

generated under the same experimental conditions [49]. For randomly distributed CO_2, Vozzi *et al.* [22] reported that there was no minimum found in HHG spectra using an 800-nm laser. However, for the 1300-nm lasers, the data from Torres *et al.* [23,67] appeared to show a very weak minimum at photon energy near 45 eV. Without more careful study including different intensities and wavelengths, however, this is not conclusive.

B. HHG spectra of aligned CO_2: Theory versus experiment

Experimentally, HHG spectra have also been reported from aligned CO_2 molecules. A relatively weak and short laser pulse was used to impulsively align molecules, and the HHG spectra were taken at half revival ($\sim$21.2 ps in CO_2) when the molecules were maximally aligned [49]. The angular distributions of the aligned molecules are obtained by solving the TDSE of the rotational wave packet [58]. The degree of alignment is $\langle\cos^2\theta\rangle = 0.60$ in Fig. 1(d), and $\langle\cos^2\theta\rangle = 0.50$ in Figs. 1(e) and 1(f). The polarizations of the pump and probe lasers are parallel to each other.

The HHG spectra of partially aligned CO_2 molecules are shown in Figs. 1(d)–1(f), and are obtained under the same generating lasers and experimental arrangements as those in Figs. 1(a)–1(c), respectively. The simulation and experimental data agree well with each other in general. In Fig. 1(e), the discrepancy is a little bigger, showing the drop near 40 eV is larger in the experiment than in the theory. But we note that in Fig. 1(f), the experimental data do not drop as rapidly, in agreement with the theoretical simulation.

The minima in the HHG spectra of CO_2 and their dependence on laser intensity have been widely discussed in the literature [21,23]. In Fig. 1(d), for an 800-nm laser, the experiment gives a strong minimum at 42 ± 2 eV, and our simulation predicts a minimum around 42 eV. For the 1200-nm laser, in Fig. 1(e), the experiment shows a minimum at 51 ± 2 eV, and theory predicts a minimum around 50 eV. In Fig. 1(f), the experimental minimum is shifted to 57 ± 2 eV, and the theoretical one is moved to around 53.5 eV. Thus our simulation also shows the shift of the minimum from low to high harmonic orders as laser intensity is increased. Below we interpret the origin of the shift.

C. Origin of minimum in the HHG spectra of aligned CO_2: Type I and type II

We next analyze the origin of the minimum in the HHG spectra seen in Figs. 1(d)–1(f), and consider the dominant contributions from the HOMO and HOMO-2 only. First, we define the averaged PR transition dipole for each molecular orbital by

$$d^{\parallel,\mathrm{avg}}(\omega,\alpha) = \int_0^\pi N(\theta)^{1/2} d^{\parallel}(\omega,\theta)\rho(\theta,\alpha)\sin\theta d\theta. \quad (13)$$

This gives a measure of the relative contribution of each molecular orbital to the HHG, which is obtained by averaging over the angular (or alignment) distribution of the partially

aligned molecules, weighted by the square root of the tunneling ionization probability. The relative ionization rates between the HOMO and HOMO-2 change with laser intensity.

Figures 2(a)–2(c) show the envelopes of the HHG spectra from individual molecular orbitals together with the total ones, each obtained after propagation in the medium. Meanwhile, the averaged PR transition dipoles of the HOMO and HOMO-2 under different generating lasers and alignment distributions are shown in Figs. 2(d)–2(f), respectively.

In Figs. 2(a) and 2(b), there are no minima in the HHG spectra of the HOMO or HOMO-2, but the minimum shows up in the total spectra. This is due to the interference between the HOMO and HOMO-2. We call this type I minimum. Clearly the minimum position will change with laser intensity since the relative ionization rates between the HOMO and HOMO-2 change with intensity [also see Figs. 5(c) and 5(d)]. A similar analysis can be found in Ref. [21]. In Fig. 2(c), there is a minimum in the HOMO spectra at 52.6 eV. This minimum is shifted to 53.6 eV in the total spectra due to the interference with the HOMO-2. This is categorized as type II minimum. A similar analysis of this type can be found in Refs. [23,68]. The minimum in the HOMO spectra is due to the minimum in the averaged PR transition dipole of the HOMO shown in Fig. 2(f). But their positions differ due to modification of the macroscopic wave packet (MWP). In this connection, we mention that the earlier calculations [34,35] with an 800-nm laser showed the minimum in HHG spectra at small pump-probe angles due to the contribution from the HOMO only. These calculations were carried out with a higher degree of alignment and higher laser intensities compared to our present study. This is expected as the minimum in the averaged PR transition dipole from the HOMO in Fig. 2(d) becomes deeper and is slightly shifted away from the cutoff to lower energies with an increased degree of alignment [see Figs. 2(e) and 2(f)]. Furthermore, as shown in Ref. [55], the minimum in the HOMO spectra could also result from the multiplication of the MWP and the averaged PR transition dipole, even when neither has the minimum. When a minimum occurs in the dominant orbital, its position will not change much if it remains the dominant one when the laser intensity changes. The little bump around 36 eV in the HOMO spectra as well as in the total spectra can be seen due to the bump in the HOMO curves in Figs. 2(d)–2(f). Its position does not change much since the HOMO-2 remains small.

Previously in Refs. [8,55], we have shown that the macroscopic HHG spectrum is the product of a MWP and an averaged PR transition dipole for each individual molecular orbital. Since the ionization rate for each orbital has been incorporated in the averaged PR transition dipole, the MWP is mostly identical, except for the phase due to ionization potential. The averaged PR transition dipole is very sensitive to ionization rates. The relative magnitude changes rapidly with the increase of laser intensity. Thus when two averaged PR transition dipoles are comparable [see Fig. 2(d)], the position of the minimum changes rapidly with the laser intensity. The averaged PR transition dipole is also sensitive to alignment distributions [see Figs. 2(d)–2(f)]. At low laser intensity, the HOMO-2 is small, and interference often occurs in a narrow region only where the two amplitudes are comparable; see Figs. 2(b) and 2(c). In comparison, in Smirnova *et al.* [21],

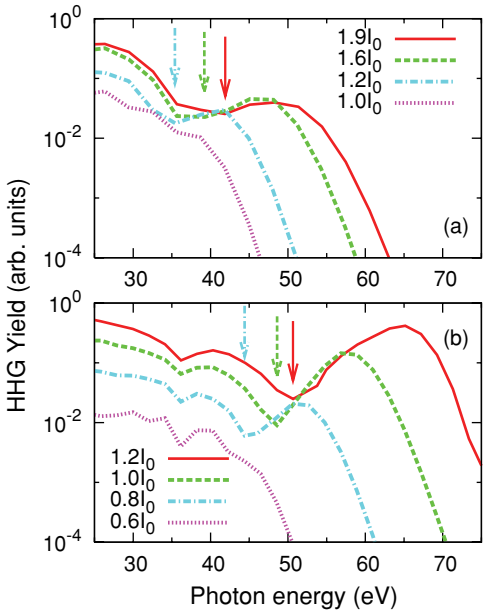

FIG. 3. (Color online) Laser-intensity dependence of macroscopic HHG spectra (envelope only) in (a) an 800-nm laser and (b) a 1200-nm laser. Intensities are shown in units of $I_0 = 10^{14}$ W/cm^2. Arrows indicate the positions of minima. Degree of alignment is $\langle \cos^2 \theta \rangle = 0.60$. Pump-probe angle $\alpha = 0^\circ$.

the HOMO and HOMO-2 tend to interfere over a broad photon-energy region. The ionization rates and transition dipoles used in their calculations are different from ours.

D. Progression of harmonic minimum versus laser intensity

In Figs. 3(a) and 3(b), we show the envelope of the calculated HHG spectra for four different peak intensities with an 800-nm laser and a 1200-nm laser, respectively. For the 800-nm spectra, the lowest intensity does not have a minimum. For the higher ones, each spectrum has a type I minimum, with position shifts to lower photon energy as the laser intensity is decreased. The degree of alignment of molecules used in the calculation is $\langle \cos^2 \theta \rangle = 0.60$. We find that the shift cannot be attributed to either the MWP or the averaged PR transition dipole alone. For the 1200-nm data, also with $\langle \cos^2 \theta \rangle = 0.60$, which is different from Figs. 1(e) and 1(f), we find that the minimum is type II, where the averaged PR transition dipole of the HOMO has a minimum. The minimum in the HHG spectra of the HOMO shifts to higher photon energy as the intensity increases, but the interference with the HOMO-2 shifts the minimum to even higher energies. In other words, the shift of the position of the HHG minimum versus intensity cannot be attributed to a single factor alone.

E. Other factors that influence the precise positions of HHG minima

In our analysis, the averaged PR transition dipole is calculated over the angular distribution of the molecules and thus depends on the degrees of alignment. Since the latter cannot be accurately measured, we check how sensitive the calculated spectra is with respect to the assumed alignment distribution. In Fig. 4(c), four different alignment distributions

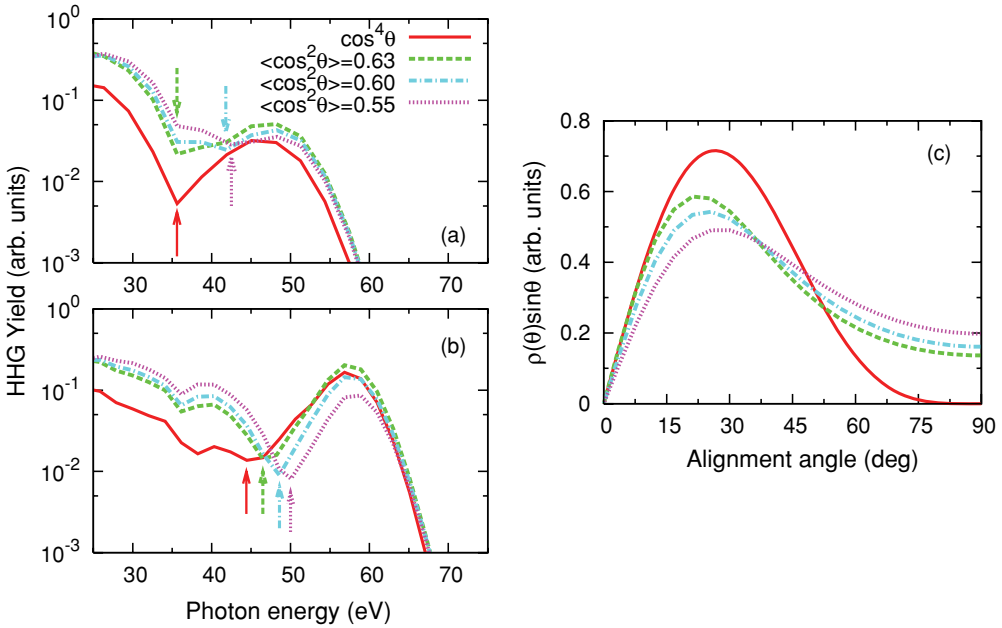

FIG. 4. (Color online) Dependence of macroscopic HHG spectra (envelope only) with degrees of molecular alignment distributions for (a) an 800-nm laser with intensity of 1.8×10^{14} W/cm^2, and (b) a 1200-nm laser with intensity of 1.0×10^{14} W/cm^2. (c) Weighted angular distributions of the molecules. Arrows indicate the positions of minima. Pump-probe angle $\alpha = 0^\circ$.

are shown. The distributions are multiplied by the volume element $\sin\theta$ for easy comparison. Three of them are obtained from the calculated rotational wave packets [58], with $\langle\cos^2\theta\rangle$ as 0.63, 0.60, and 0.55, respectively. The other is the commonly used $\cos^4\theta$ distribution. For 800-nm and 1200-nm lasers, the envelopes of the calculated HHG spectra are shown in Figs. 4(a) and 4(b), respectively. The precise position of the minimum changes slightly, except for the one from the $\cos^4\theta$ distributions. However, a change of a couple of electron volts is seen.

To precisely determine the minimum in the HHG spectra, the accurate alignment-dependent ionization probability $N(\theta)$

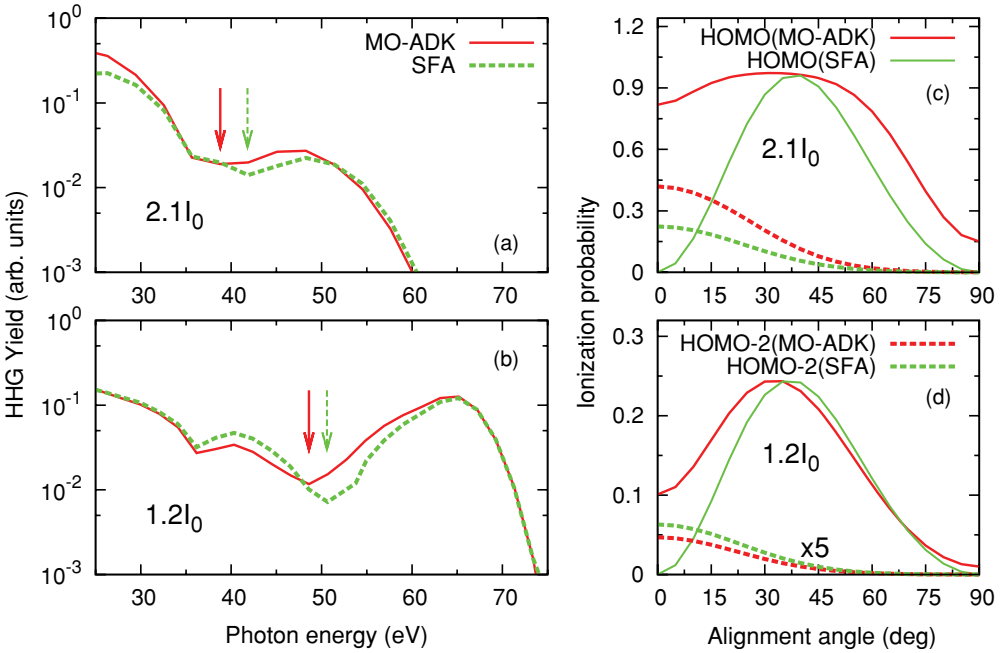

FIG. 5. (Color online) Dependence of macroscopic HHG spectra (envelope only) on the ionization probabilities calculated from the MO-ADK theory or SFA in (a) an 800-nm laser, and (b) a 1200-nm laser. Laser intensities are indicated where $I_0 = 10^{14}$ W/cm^2. Arrows indicate the positions of minima. Degree of alignment is $\langle\cos^2\theta\rangle = 0.60$. Pump-probe angle $\alpha = 0^\circ$. (c) and (d) Alignment-dependent ionization probabilities of the HOMO and HOMO-2 calculated using the MO-ADK theory and SFA. Laser parameters are the same as (a) and (b). Ionization probabilities of the HOMO-2 in (d) are multiplied by 5.

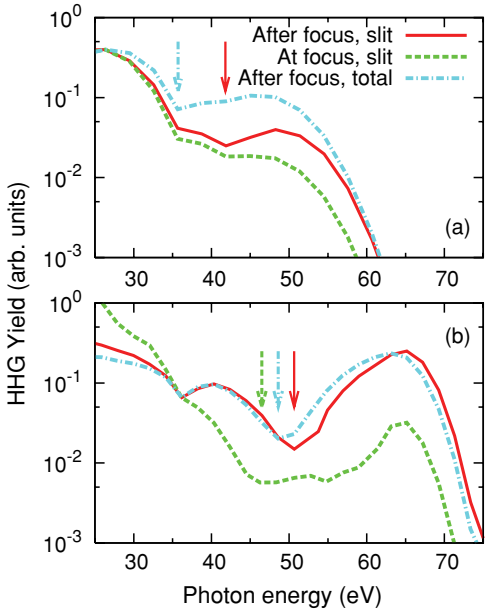

FIG. 6. (Color online) Dependence of macroscopic HHG spectra (envelope only) on experimental arrangements (a) for an 800-nm laser with intensity of 2.1×10^{14} W/cm^2, and (b) for a 1200-nm laser with intensity of 1.2×10^{14} W/cm^2. The arrangements are (1) gas jet after focus and slit is used (solid lines), (2) gas jet at the focus and slit is used (dashed lines), and (3) gas jet after the focus but without the slit (dot-dashed lines). Arrows indicate the positions of minima. Degree of alignment is $\langle \cos^2 \theta \rangle = 0.60$. Pump-probe angle $\alpha = 0°$.

for each molecular orbital is needed. For CO_2, and even for the HOMO, different theories in the literature [21,40–43,45–47] show non-negligible differences, and they do not agree with the experimental data [41]. Here we examine how the HHG spectra change with the different ionization rates used. The ionization rates for both the HOMO and HOMO-2 can all be easily calculated from SFA or from the MO-ADK theory. Figures 5(a) and 5(b) show the HHG spectra calculated using the ionization probabilities shown in Figs. 5(c) and 5(d). Other laser parameters used in the calculation are given in the figure captions. The difference of the position of the minimum is 3 eV in Fig. 5(a) and 2 eV in Fig. 5(b). Note that the ionization probabilities from SFA and the MO-ADK theory are normalized at the peak of the HOMO curve. In Fig. 5(a), the spectra are normalized at H33 (51 eV), and in Fig. 5(b), at H65 (67 eV).

The HHG spectra are also sensitive to the experimental arrangement and thus can also move the position of the HHG minimum. To demonstrate this, we (i) move the gas jet to the laser focus and collect the HHG signal using a slit, and (ii) put the gas jet after the laser focus and collect the HHG signal without a slit (total signal). These two will be compared to the arrangement used in this paper, in which the gas jet is put after the laser focus and the HHG is collected with a slit. The results are compared in Fig. 6. Note that the spectra are normalized at H17 (26 eV) in Fig. 6(a) and at H35 (36 eV) in Fig. 6(b). Not only do the spectra change quite significantly, but the position of the HHG minimum changes also. This illustrates that it is very difficult to compare the position of the HHG minimum from different experiments. In this comparison, the change of the HHG

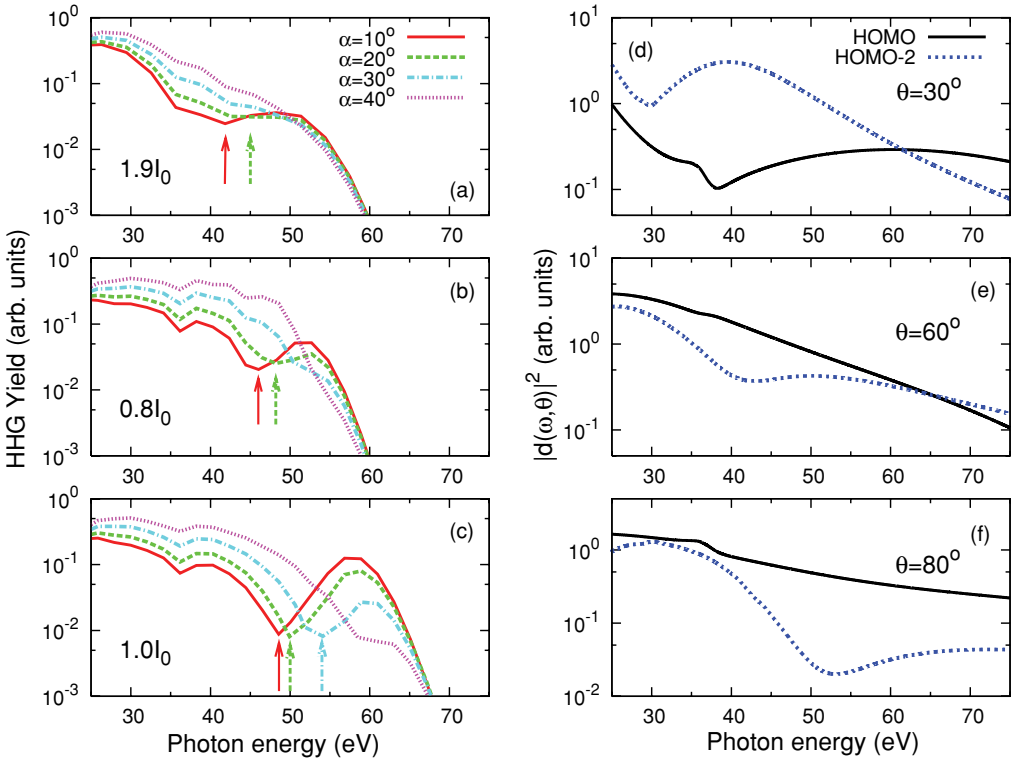

FIG. 7. (Color online) Dependence of macroscopic HHG spectra (envelope only) on pump-probe angles $\alpha = 10°$, $20°$, $30°$, and $40°$ for (a) an 800-nm laser, and (b), (c) for a 1200-nm laser. Laser intensities are given in units of $I_0 = 10^{14}$ W/cm^2. Arrows indicate the positions of minima. Degree of alignment is $\langle \cos^2 \theta \rangle = 0.60$ ($\alpha = 0°$). (d)–(f) Photorecombination transition dipoles (parallel component, the square of magnitude) of the HOMO and HOMO-2 in terms of photon energy at alignment angles $\theta = 30°$, $60°$, and $80°$.

spectra is due to the change of the MWP, which depends on the experimental setup. The averaged PR transition dipoles of the HOMO and HOMO-2 are the same in the three calculations.

F. The dependence of the HHG minimum on the pump-probe angle

In Wörner *et al.* [49], it was found that the minimum in the HHG spectra of aligned CO_2 moved to higher photon energy with increasing pump-probe angle α, i.e., the angle between the aligning pump beam and the HHG-generating probe-beam polarizations. This phenomenon has also been observed in other measurements [21,69]. In contrast, the minimum in the HHG spectra of aligned N_2 has been found to stay at the same position for all pump-probe angles [14,69].

We show the calculated HHG spectra at four pump-probe angles in an 800-nm laser in Fig. 7(a), and in a 1200-nm laser in Figs. 7(b) and 7(c). Laser parameters and experimental arrangements are the same as in Fig. 1, and the degree of alignment is $\langle \cos^2 \theta \rangle = 0.60$ ($\alpha = 0^\circ$). The HHG spectra for $\alpha = 0^\circ$ have been shown in Fig. 3. These figures show that the minimum in the HHG spectra moves to higher photon energies with increasing α, and the minimum disappears at large angles. At larger pump-probe angles, contributions from large alignment angles increase. The HOMO dominates over the HOMO-2 at large angles in both the ionization rates [see Figs. 5(c) and 5(d)] and the PR transition dipoles [see Figs. 7(d)–7(f)], thus HHG at large pump-probe angles has essentially no contributions from the HOMO-2. Also note that at small α, the total HHG yield is much smaller [34]. In fact, the total HHG spectra for randomly distributed CO_2 have little contributions from molecules that are aligned nearly parallel to the polarization axis of the laser. The HHG spectra of CO_2 are complex only in the region where HHG yields are small. This is generally true—the interpretation of small processes always requires careful and detailed theories.

IV. SUMMARY AND OUTLOOK

In this paper we have analyzed the multiple orbital contribution to HHG in CO_2 with the inclusion of the macroscopic propagation effect. In the past few years, there have been many experimental and theoretical studies on the HHG of CO_2 from many laboratories, using lasers with different wavelengths and intensities, for CO_2 molecules that are randomly distributed or partially aligned. In particular, for CO_2 molecules that are partially aligned along the polarization axis of the probe laser, many experiments have shown that the HHG spectra exhibit minima and the positions of the minima shift with laser intensities [21,23,49]. The shift of the minimum position with laser intensities has been attributed to the interference between the contributions to HHG from the HOMO-2 with the one from the HOMO, despite the HOMO-2 lying 4.4 eV deeper than the HOMO. Since HHG is a nonlinear process, these observations pose a great challenge to the theory, especially for the prediction of the position of the minimum and how it changes with the experimental conditions. Since all experimental HHG spectra include the macroscopic propagation effect, a comparison of theory with experiment is incomplete unless the theory also has included the propagation effect. Our analysis in this paper is based on the macroscopic propagation code extended for aligned molecules, and the recently developed quantitative rescattering theory. We find that although HHG spectra change significantly under different experimental parameters such as degree of alignment, focusing condition, and the use of a slit, the position of the minimum in the HHG spectra behaves in a similar trend as laser intensity and pump-probe angle vary. This trend has been found to be consistent with the recent experimental measurements from different groups.

We comment that the present theory and the earlier one by Smirnova *et al.* [21] both explain the intensity dependence of the change of HHG minima, but the details between the two theories are quite different. The alignment dependence of the ionization rates, the recombination dipole matrix elements, and their phases entering the two theories are not the same, for both the HOMO and HOMO-2. As illustrated in this paper, these parameters can all affect the position of the predicted interference minimum. Furthermore, in Smirnova *et al.* [21], the interference is attributed to the importance of hole dynamics in the ion core. Our approach is formulated in the time-independent fashion, and no hole dynamics is included. Since HHG spectra are taken without the explicit observation of electron dynamics, the difference between the two models cannot be settled. Despite these differences, our understanding of the HHG spectra of CO_2 has come a long way since 2005 [26]. With the possibility of including the macroscopic propagation effect "routinely" in the HHG theory for molecular targets, further experimental studies should explore the effects of the laser-focusing condition and gas pressure for lasers extending to longer wavelengths. Such studies would further our basic understanding of the strong-field physics of molecules to the next level, and eliminate the need to introduce extraneous assumptions in the interpretation of experimental data.

ACKNOWLEDGMENTS

This work was supported in part by Chemical Sciences, Geosciences and Biosciences Division, Office of Basic Energy Sciences, Office of Science, US Department of Energy.

[1] C. Winterfeldt, C. Spielmann, and G. Gerber, Rev. Mod. Phys. **80**, 117 (2008).
[2] T. Brabec and F. Krausz, Rev. Mod. Phys. **72**, 545 (2000).
[3] P. Agostini and L. F. DiMauro, Rep. Prog. Phys. **67**, 813 (2004).
[4] M. B. Gaarde, J. L. Tate, and K. J. Schafer, J. Phys. B **41**, 132001 (2008).
[5] E. Priori, G. Cerullo, M. Nisoli, S. Stagira, S. De Silvestri, P. Villoresi, L. Poletto, P. Ceccherini, C. Altucci, R. Bruzzese, and C. de Lisio, Phys. Rev. A **61**, 063801 (2000).

[6] V. Tosa, H. T. Kim, I. J. Kim, and C. H. Nam, Phys. Rev. A **71**, 063807 (2005).
[7] M. Geissler, G. Tempea, A. Scrinzi, M. Schnürer, F. Krausz, and T. Brabec, Phys. Rev. Lett. **83**, 2930 (1999).
[8] C. Jin, A. T. Le, and C. D. Lin, Phys. Rev. A **83**, 023411 (2011).
[9] C. Altucci *et al.*, Phys. Rev. A **73**, 043411 (2006).
[10] M. C. H. Wong, J.-P. Brichta, and V. R. Bhardwaj, Phys. Rev. A **81**, 061402 (2010).
[11] M. C. H. Wong, J.-P. Brichta, and V. R. Bhardwaj, Opt. Lett. **35**, 1947 (2010).
[12] C. Trallero-Herrero *et al.*, Chem. Phys. **366**, 33 (2009).
[13] B. K. McFarland, J. P. Farrell, P. H. Bucksbaum, and M. Gühr, Science **322**, 1232 (2008).
[14] S. Haessler *et al.*, Nature Phys. **6**, 200 (2010).
[15] Y. Mairesse *et al.*, Phys. Rev. Lett. **104**, 213601 (2010).
[16] G. H. Lee, I. J. Kim, S. B. Park, T. K. Kim, Y. S. Lee, and C. H. Nam, J. Phys. B **43**, 205602 (2010).
[17] W. Boutu *et al.*, Nature Phys. **4**, 545 (2008).
[18] T. Kanai, E. J. Takahashi, Y. Nabekawa, and K. Midorikawa, Phys. Rev. A **77**, 041402 (2008).
[19] N. Wagner, X. Zhou, R. Lock, W. Li, A. Wüest, M. Murnane, and H. Kapteyn, Phys. Rev. A **76**, 061403 (2007).
[20] X. Zhou, R. Lock, W. Li, N. Wagner, M. M. Murnane, and H. C. Kapteyn, Phys. Rev. Lett. **100**, 073902 (2008).
[21] O. Smirnova, Y. Mairesse, S. Patchkovskii, N. Dudovich, D. Villeneuve, P. Corkum, and M. Yu. Ivanov, Nature (London) **460**, 972 (2009).
[22] C. Vozzi *et al.*, Phys. Rev. Lett. **95**, 153902 (2005).
[23] R. Torres *et al.*, Phys. Rev. A **81**, 051802 (2010).
[24] P. B. Corkum, Phys. Rev. Lett. **71**, 1994 (1993).
[25] J. L. Krause, K. J. Schafer, and K. C. Kulander, Phys. Rev. Lett. **68**, 3535 (1992).
[26] T. Kanai, S. Minemoto, and H. Sakai, Nature (London) **435**, 470 (2005).
[27] M. Lein, N. Hay, R. Velotta, J. P. Marangos, and P. L. Knight, Phys. Rev. Lett. **88**, 183903 (2002).
[28] A. T. Le, X. M. Tong, and C. D. Lin, Phys. Rev. A **73**, 041402 (2006).
[29] M. Lewenstein, Ph. Balcou, M. Yu. Ivanov, A. L'Huillier, and P. B. Corkum, Phys. Rev. A **49**, 2117 (1994).
[30] X. X. Zhou, X. M. Tong, Z. X. Zhao, and C. D. Lin, Phys. Rev. A **71**, 061801 (2005).
[31] X. X. Zhou, X. M. Tong, Z. X. Zhao, and C. D. Lin, Phys. Rev. A **72**, 033412 (2005).
[32] C. D. Lin, A. T. Le, Z. Chen, T. Morishita, and R. R. Lucchese, J. Phys. B **43**, 122001 (2010).
[33] T. Morishita, A. T. Le, Z. Chen, and C. D. Lin, Phys. Rev. Lett. **100**, 013903 (2008).
[34] A. T. Le, R. R. Lucchese, S. Tonzani, T. Morishita, and C. D. Lin, Phys. Rev. A **80**, 013401 (2009).
[35] A. T. Le, R. R. Lucchese, M. T. Lee, and C. D. Lin, Phys. Rev. Lett. **102**, 203001 (2009).
[36] A. T. Le, R. R. Lucchese, and C. D. Lin, Phys. Rev. A **82**, 023814 (2010).
[37] D. W. Turner, C. Baker, A. D. Baker, and C. R. Brundle, *Molecular Photoelectron Spectroscopy: A Handbook of He 584 Å Spectra* (Wiley, London, 1970).
[38] C. D. Lin, X. M. Tong, and Z. X. Zhao, J. Mod. Opt. **53**, 21 (2006).
[39] X. M. Tong, Z. X. Zhao, and C. D. Lin, Phys. Rev. A **66**, 033402 (2002).
[40] S. F. Zhao, C. Jin, A. T. Le, T. F. Jiang, and C. D. Lin, Phys. Rev. A **81**, 033423 (2010).
[41] D. Pavičić, K. F. Lee, D. M. Rayner, P. B. Corkum, and D. M. Villeneuve, Phys. Rev. Lett. **98**, 243001 (2007).
[42] V.-H. Le, N.-T. Nguyen, C. Jin, A.-T. Le, and C. D. Lin, J. Phys. B **41**, 085603 (2008).
[43] M. Spanner and S. Patchkovskii, Phys. Rev. A **80**, 063411 (2009).
[44] S. F. Zhao, C. Jin, A. T. Le, T. F. Jiang, and C. D. Lin, Phys. Rev. A **80**, 051402 (2009).
[45] M. Abu-samha and L. B. Madsen, Phys. Rev. A **80**, 023401 (2009).
[46] S. K. Son and Shih-I. Chu, Phys. Rev. A **80**, 011403 (2009).
[47] S. Petretti, Y. V. Vanne, A. Saenz, A. Castro, and P. Decleva, Phys. Rev. Lett. **104**, 223001 (2010).
[48] A. T. Le, R. R. Lucchese, and C. D. Lin, J. Phys. B **42**, 211001 (2009).
[49] H. J. Wörner, J. B. Bertrand, P. Hockett, P. B. Corkum, and D. M. Villeneuve, Phys. Rev. Lett. **104**, 233904 (2010).
[50] M. B. Gaarde, M. Murakami, and R. Kienberger, Phys. Rev. A **74**, 053401 (2006).
[51] M. B. Gaarde and K. J. Schafer, Phys. Rev. A **65**, 031406 (2002).
[52] A. T. Le, R. D. Picca, P. D. Fainstein, D. A. Telnov, M. Lein, and C. D. Lin, J. Phys. B **41**, 081002 (2008).
[53] S. F. Zhao, C. Jin, R. R. Lucchese, A. T. Le, and C. D. Lin, Phys. Rev. A **83**, 033409 (2011).
[54] C. Jin, A. T. Le, and C. D. Lin, Phys. Rev. A **79**, 053413 (2009).
[55] C. Jin, H. J. Wörner, V. Tosa, A. T. Le, J. B. Bertrand, R. R. Lucchese, P. B. Corkum, D. M. Villeneuve, and C. D. Lin, J. Phys. B **44**, 095601 (2011).
[56] J. P. Farrell, L. S. Spector, B. K. McFarland, P. H. Bucksbaum, M. Gühr, M. B. Gaarde, and K. J. Schafer, Phys. Rev. A **83**, 023420 (2011).
[57] J. Higuet *et al.*, Phys. Rev. A **83**, 053401 (2011).
[58] C. Jin, A. T. Le, S. F. Zhao, R. R. Lucchese, and C. D. Lin, Phys. Rev. A **81**, 033421 (2010).
[59] M. Lein *et al.*, J. Mod. Opt. **52**, 465 (2005).
[60] A. E. Siegman, *Lasers* (University Science, Mill Valley, CA, 1986).
[61] A. L'Huillier, Ph. Balcou, S. Candel, K. J. Schafer, and K. C. Kulander, Phys. Rev. A **46**, 2778 (1992).
[62] V. Tosa, K. T. Kim, and C. H. Nam, Phys. Rev. A **79**, 043828 (2009).
[63] R. R. Lucchese and V. McKoy, Phys. Rev. A **26**, 1406 (1982).
[64] R. R. Lucchese, G. Raseev, and V. McKoy, Phys. Rev. A **25**, 2572 (1982).
[65] C. B. Madsen and L. B. Madsen, Phys. Rev. A **74**, 023403 (2006).
[66] C. Figueira de Morisson Faria and B. B. Augstein, Phys. Rev. A **81**, 043409 (2010).
[67] R. Torres *et al.*, Opt. Express **18**, 3174 (2010).
[68] O. Smirnova, S. Patchkovskii, Y. Mairesse, N. Dudovich, and M. Yu. Ivanov, Proc. Natl. Acad. Sci. USA **106**, 16556 (2009).
[69] Y. Mairesse, J. Levesque, N. Dudovich, P. B. Corkum, and D. M. Villeneuve, J. Mod. Opt. **55**, 2591 (2008).